11. Stöhr, J. *et al.* Element specific magnetic microscopy with circularly polarized X-rays. *Science* **259,** 658–661 (1993).
12. Takano, K. *et al.* Interfacial uncompensated antiferromagnetic spins: role of unidirectional anisotropy in polycrystalline $Ni_{81}Fe_{19}$/CoO bilayers. *Phys. Rev. Lett.* **79,** 1130–1133 (1997).
13. Eibschütz, M., Shtrikman, S. & Treves, D. Mössbauer studies of Fe^{57} in orthoferrites. *Phys. Rev.* **156,** 562–577 (1967).

Acknowledgements

This work was supported by the Director, Office of Basic Energy Sciences, of the US Department of Energy. J.W.S. and F.N. acknowledge support by the Swiss National Science Foundation.

Correspondence and requests for materials should be addressed to F.N. (e-mail: FNolting@lbl.gov).

Reversible electromechanical characteristics of carbon nanotubes under local-probe manipulation

Thomas W. Tombler*, Chongwu Zhou*, Leo Alexseyev*, Jing Kong*, Hongjie Dai*, Lei Liu†, C. S. Jayanthi†, Meijie Tang‡ & Shi-Yu Wu†

* *Department of Chemistry, Stanford University, Stanford, California 94305, USA*
† *Department of Physics, University of Louisville, Louisville, Kentucky 40292, USA*
‡ *Physics Directorate, Lawrence Livermore National Laboratory, Livermore, California 94551, USA*

The effects of mechanical deformation on the electrical properties of carbon nanotubes are of interest given the practical potential of nanotubes in electromechanical devices, and they have been studied using both theoretical[1–4] and experimental[5,6] approaches. One recent experiment[6] used the tip of an atomic force microscope (AFM) to manipulate multi-walled nanotubes, revealing that changes in the sample resistance were small unless the nanotubes fractured or the metal–tube contacts were perturbed. But it remains unclear how mechanical deformation affects the intrinsic electrical properties of nanotubes. Here we report an experimental and theoretical elucidation of the electromechanical characteristics of individual single-walled carbon nanotubes (SWNTs) under local-probe manipulation. We use AFM tips to deflect suspended SWNTs reversibly, without changing the contact resistance; *in situ* electrical measurements reveal that the conductance of an SWNT sample can be reduced by two orders of magnitude when deformed by an AFM tip. Our tight-binding simulations indicate that this effect is owing to the formation of local sp^3 bonds caused by the mechanical pushing action of the tip.

We prepared samples of individual SWNTs bridging metal electrodes on SiO_2/Si substrates[7–9], with part of the SWNT length suspended over trenches fabricated on the SiO_2 surface (Fig. 1a). We characterized the partially suspended individual SWNTs by AFM imaging. Figure 1b shows the AFM image of an SWNT with suspended length $l \approx 605$ nm over a trench. The image was obtained by tapping-mode AFM (TM-AFM) with the tip scanning direction parallel to the tube axis. Figure 1c shows the experimental setup for bending a suspended SWNT mechanically with an AFM tip while measuring the nanotube electrical properties.

After a desired SWNT device was located and imaged by TM-AFM, the AFM tip was positioned above the centre of the suspended nanotube. The nanotube suspension was pushed towards the bottom of the trench by moving the sample-stage upward. The stage was then retracted. The pushing–retracting cycle was repeated many times, during which the AFM cantilever deflection and the resistance of the SWNT sample were simultaneously recorded as a function of time. This approach allowed repeated measurements of resistance versus nanotube deflection, as the cantilever deflection signal (ΔZ_c) can readily be converted into the deflection of the suspended nanotube at its centre point (ΔZ_T, Fig. 1c). By controlling the initial tip–tube distance Z_0 and the total sample-stage travel range (Z_{range}), we were able to deflect the suspended SWNT to various degrees and study the effect of mechanical deformation on the electrical properties of SWNTs.

Figure 2 shows cantilever deflection ΔZ_c versus vertical coordinate Z recorded during one cycle of pushing on the suspended SWNT sample shown in Fig. 1b. Beyond the tip-tube contact point $Z_0 \approx 50$ nm, the vertical deflection occurring at the centre of the suspended SWNT is $\delta(Z) = \Delta Z_T(Z) = (Z - Z_0) - \Delta Z_c(Z)$, and the force applied to the nanotube is $F(\delta) = k_c \Delta Z_c(\delta)$. We find that the force $F(\delta)$ versus nanotube deflection δ curve (Fig. 2, inset) right after the tube-tip contact can be fitted well into $F(\delta) = 8YA(\delta/l)^3$,

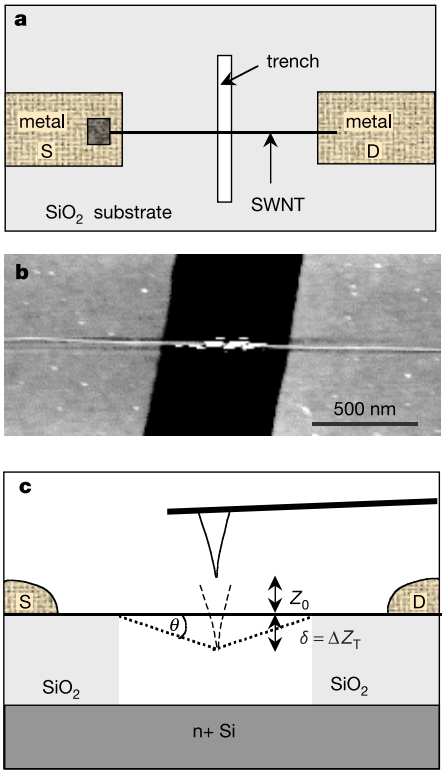

Figure 1 An SWNT partly suspended over a trench for electromechanical measurements. **a**, Device viewed from above. Preparation of samples involves chemical vapour deposition of SWNTs at desired surface sites using SiO_2/Si substrates with patterned catalyst islands[7–9]. The substrates contain trenches that are about 500 nm wide and 175 nm deep, pre-fabricated next to patterned catalyst islands (dark square). Thus, the SWNT bridging a pair of metal electrodes (S is the source, D is the drain) is partly suspended over the trench. The spacing between metal electrodes is about 3–4 μm. The metal used to contact SWNTs is 20 nm thick Ti and 60 nm Au placed on top of the SWNTs over a contact length of about 1 μm. **b**, AFM image of an SWNT with suspended length $l \approx 605$ nm. The cantilever employed for this experiment has a spring constant $k_c = 0.6\ N\ m^{-1}$. The integrated tip on the cantilever is pyramidal with tip radius of about 10–15 nm. The bright streaks around the suspended tube are caused by tube touching and sticking to the side of the pyramid when the tip is scanned near the tube. The diameter of the SWNT $d = 3.1 \pm 0.2$ nm, measured from the apparent height of the nanotube resting on the SiO_2 surface. The nanotube is a relatively large diameter SWNT synthesized by our chemical vapour deposition approach[7]. It could also be a small SWNT bundle, but this should not change our main conclusions. **c**, Side-view of the AFM pushing experiment. The tip is centred above the SWNT suspension by slowly zooming into the tube-suspension during real-space imaging.

where $A = (\pi d)t$ (where $t = 3.4$ Å, van der Waals wall thickness) is the nanotube cross-section area. This yields a Young's modulus of the nanotube $Y \approx 1.2$ TPa, similar to previous results $Y = 0.6 - 1.3$ TPa for SWNTs[10]. The $F(\delta) \propto \delta^3$ fitting indicates that the suspended SWNT can be considered as an elastic string when it is under initial force loading at the centre[11,12]. Assuming that the deflected SWNT is pivoted at the edges of the trench and forms a triangle with its original configuration (Fig. 1c), we define $\sigma = [(4\delta^2 + l^2)^{1/2} - l]/l$ as a global strain parameter distributed over the length of the nanotube. Alternatively, a parameter $\theta = \tan^{-1}(2\delta/l)$ is defined as the angle between the deflected SWNT and its original configuration (Fig. 1c). For $\sigma > \sim 0.3\%$ ($\theta > \sim 5°$), the force versus deflection relation is found to deviate from $F(\delta) \propto \delta^3$ (Fig. 2).

Figure 3 shows the cantilever deflection and sample conductance evolution during repeated tip-pushing of the suspended part of the SWNT. For initial tip–tube distances $Z_0 \approx 65$ nm, 30 nm and 8 nm and sample-stage moving range $Z_{range} = 100$ nm, the maximum cantilever and tube deflections are $\Delta Z_c \sim 3$, 10 and 15 nm, and

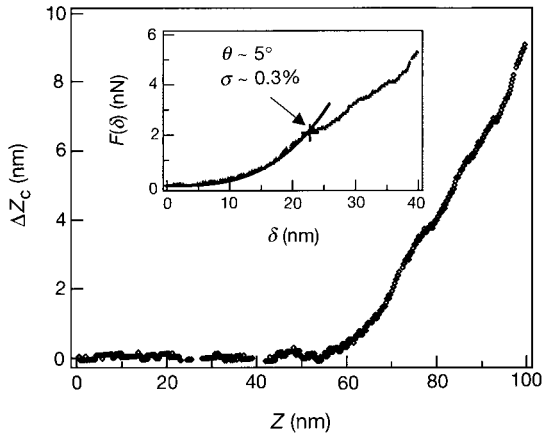

Figure 2 Cantilever deflection ΔZ_c versus vertical coordinate Z during a cycle of pushing a suspended nanotube and then retracting. Inset, force $F(\delta)$ versus nanotube deflection δ curve. Solid line: fit of $F(\delta) = 8YA(\delta/l)^3 \approx 1.53 \times 10^{14}$ (N m^{-3})δ^3. The arrow highlights the deviation point from $F \propto \delta^3$ where the tube bending angle $\theta \approx 5°$ and global strain $\sigma \approx 0.3\%$. We carried out the force–deflection analysis by first estimating a tip–tube contact point Z_0 from the ΔZ_c versus Z curve. A final Z_0 value was determined by varying Z_0 by small increments until reaching the best $F \propto \delta^3$ fit for the initial tube–tip contact regime. Such analysis allowed the determination of strain σ and bending angle θ from the cantilever deflection signal. This is useful for the characterization of nanotube electro-mechanical properties (see Figs 3 and 4).

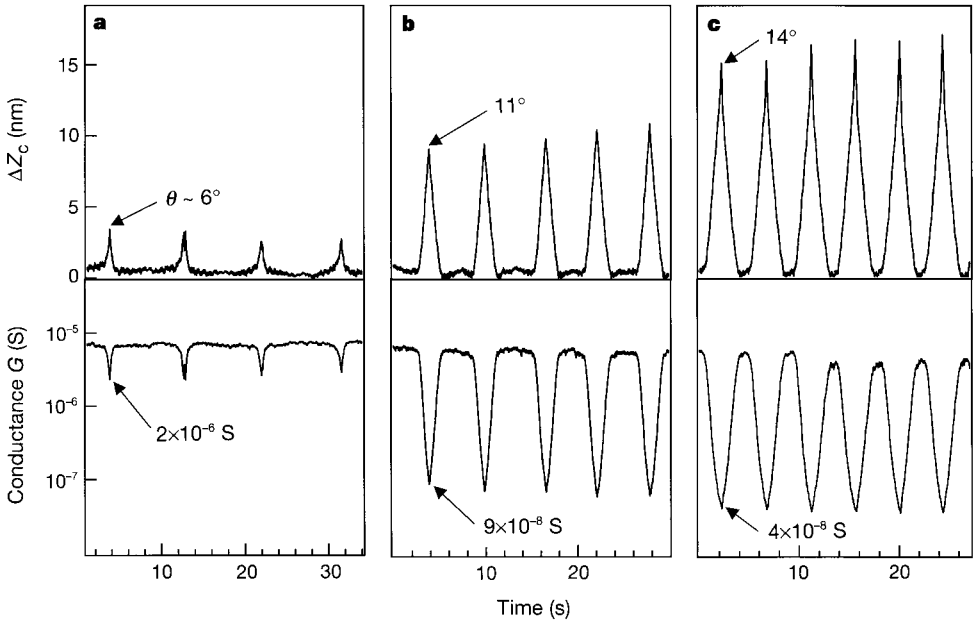

Figure 3 Cantilever deflection and nanotube electrical conductance evolution during repeated cycles of pushing the suspended SWNT. Initial tip–tube distance is $Z_0 \approx 65$ nm (**a**), 30 nm (**b**) and 8 nm (**c**). The speed of the tip motion was set to be ~ 22 nm s^{-1} (**a**), 34 nm s^{-1} (**b**) and 44 nm s^{-1} (**c**). Tip travel distance = $2Z_{range} = 200$ nm between oscillation peaks. Time resolution for the conductance measurements was 10 ms. The arrows point to the bending angles and conductance values for the first peak. The bending angles were obtained by force–deflection analysis of the three marked pushing–retracting cycles independently, using the method described in Fig. 2. The angles for the marked peaks in **a** and **b** were also evaluated based on the analysis of the marked peak in **c**. This was done by correlating the cantilever deflection values for the two peaks in **a** and **b** with the cantilever deflection versus angle curve obtained from the analysis of the marked cycle in **c**. The results were found to be consistent with the independent analyses of the marked cycles in **a** and **b**. Drifts in Z_0 (due to piezo-drifts) occurred between some of the pushing–retracting cycles, but within each cycle the drift should not be significant. Pushing the SWNT to its breaking point would provide information such as nanotube tensile strength and electrical behaviour near tube-failure. This is currently limited by the size of the trench (500 nm wide, 175 nm deep) on the samples. Note that the nanotube when unperturbed exhibited a resistance of about 200 kilo-ohms. This could be mainly contributed by contact resistance.

$\delta = \Delta Z_T \sim 30$, 60 and 76 nm, respectively (Fig. 3a–c). The conductance of the SWNT sample decreases each time the AFM tip pushes the nanotube down, but recovers as the tip retracts. The repeated pushing–retracting causes oscillations in the cantilever–nanotube deflection and sample conductance, with equal periodicity in the two oscillations. Importantly, both the mechanical deformation and electrical conductance of the nanotube are highly reversible. The full reversal of these characteristics upon tip retraction has important implications. First, reversibility in the electrical property indicates that the metal–tube contacts are not affected when the tip deflects the suspended part of the nanotube. The observed change in sample conductance is entirely owing to the mechanical deformation of the SWNT caused by the pushing tip. Secondly, reversibility in both the mechanical and electrical properties indicates that the suspended part of the SWNT is firmly pivoted at the edges of the trench. The length of the SWNT resting on the SiO_2 surface ($\geq 1.5\,\mu m$ on both sides of the trench) is not being stretched or sliding on the substrate during pushing of the suspended part. Anchoring of the nanotube on the SiO_2 substrate is attributed to strong tube–substrate van der Waals interactions[13].

The conductance of the SWNT sample decreases by more than two orders of magnitude when the AFM tip deflects the SWNT by $\delta = \Delta Z_T \approx 80$ nm (Fig. 3c). This deflection corresponds to a global strain value $\sigma \approx 3\%$ ($\theta = 14°$) in the nanotube suspension. Conductance of the SWNT sample as continuous functions of strain and bending angle are shown in Fig. 4a. The SWNT conductance decreases relatively slowly for small bending angles ($\theta \leq \sim 5°$), and the decrease becomes more dramatic at higher bending angles (Fig. 4a, inset).

To understand the physics underlying the dramatic nanotube electromechanical property, we carried out order-N non-orthogonal tight-binding molecular-dynamics simulations[14] of an AFM tip deflecting a (5,5) SWNT (960 carbon atoms, $l \approx 12$ nm). Electrical measurements with the SWNT sample described in Fig. 3 identified that the nanotube was metallic in nature, as the sample exhibited little conductance change under various back-gate voltages and remained conducting at low temperatures[5,8,9]. Therefore, we chose the (5,5) metallic tube for our simulation. The AFM tip was modelled by a capped (5,5) SWNT (110 carbon atoms). The tip was placed directly above the middle of the suspended SWNT and pushed down vertically. The simulations were carried out at 300 K. In the simulation, 40 atoms at each end of the SWNT and the 50 atoms at the top end of the tip were kept fixed. The rest of the atoms in the system were allowed to relax and reach equilibrium configuration. The conductance of the bent SWNT was calculated by the Landauer–Büttiker formula[15] using the method of real space Green's function[16]. Details of the simulations and conductance calculations will be presented elsewhere. We calculated the conductance evolution of the nanotube as it was deflected to $\theta = 0°$, 7.0°, 11°, and 15°, corresponding to $\sigma = 0$, 0.7%, 1.8%, and 3.4%, respectively (Fig. 4b). The conductance (in units of $G_0 = 2e^2/h$) at the Fermi level was found to decrease by about twofold (from 2 G_0 to $\sim$1 G_0) at $\theta = 7°$, and decrease more dramatically at larger bending angles ($G \approx 0.01\ G_0$ at $\theta = 15°$). These results are qualitatively consistent with our experimental data (Fig. 4a, inset).

Detailed analysis of our simulation results reveals that strong local bonding deformation induced by the AFM tip is responsible for the dramatic conductance decrease of the SWNT. When pushed

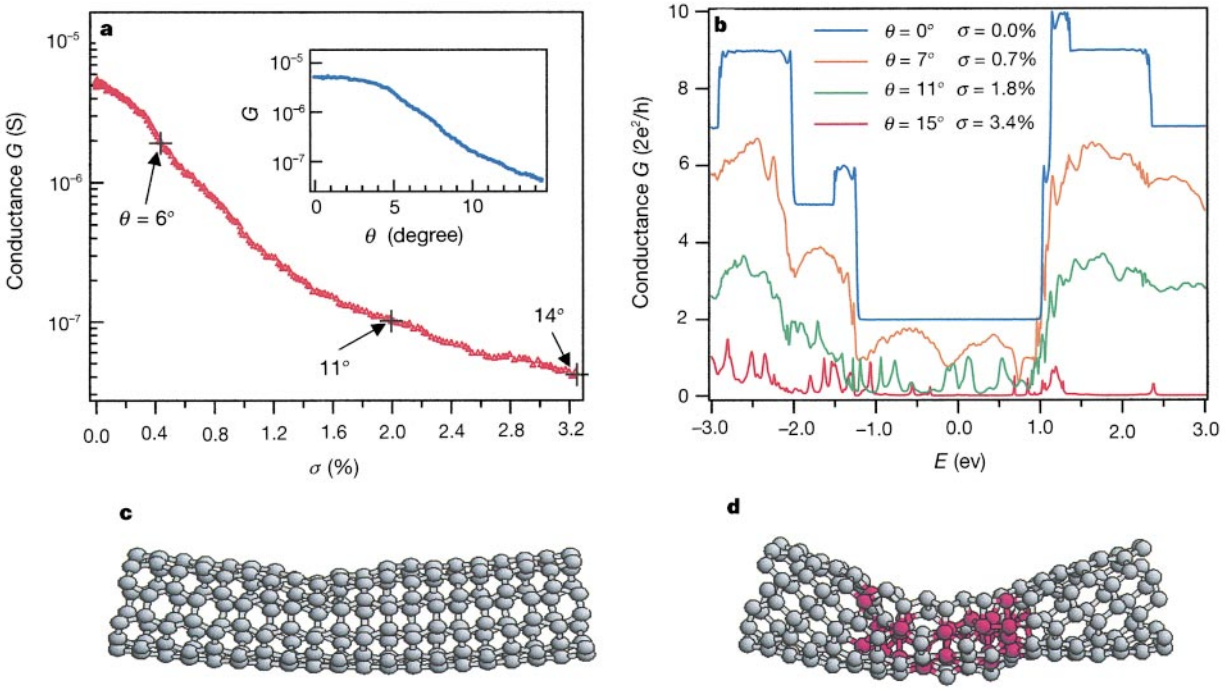

Figure 4 Electrical conductance versus mechanical deformation for a manipulated SWNT. **a**, Experimental result of conductance (G) of the SWNT sample versus strain (σ) in the suspended part of the nanotube. Inset, conductance (G) versus bending angle (θ). These data were obtained from the marked cycle in Fig. 3c. The strain (σ) does not scale linearly with θ, which accounts for the different shapes of the G–σ and G–θ curves. **b**, Conductance versus band energy calculated for an ideally contacted (5,5) SWNT under progressively larger deformation forced by a tip. The Fermi energy is at $E = 0$. The fluctuations of conductance versus energy (around E_F, for $\theta \neq 0$) are owing to variations of the transmission coefficient for different energy electrons crossing the barrier set by the large local deformation region near the tip. **c**,**d**, Simulated atomic configurations of the nanotube pushed to 7° and 15° respectively. Atoms marked in red are near the tip (not shown) and sp^3-bonded. The sp^3 bonding is found to be within the tube structure itself (between back-and-belly atoms in the nanotube). Bond number counting excludes tip-atoms. The role of the tip is to act as a forcing agent. The tip used in the experiment can be considered as a sharp point relative to the length of the tube. Also, the AFM tips typically do not have smooth textures, which may have led to a situation where the tube-tip contact is at a sharp irregular point on the tip. We measured several nanotube samples with different tips, and observed similar electromechanical properties of suspended metallic SWNTs. For instance, another SWNT (diameter $\sim$ 1.9 nm, suspended length $\sim$ 350 nm) manipulated by a different AFM tip exhibited a conductance decrease from 7×10^{-6} S to 3×10^{-6} S under $\sigma \approx 0.3\%$ and $\theta \approx 4°$.

by an AFM tip, the nanotube region proximal to the tip exhibits significant changes in atomic bonding configuration. For relatively small bending angles ($\theta \leq \sim 7°$), the nanotube retains sp^2 bonding throughout its structure. The nanotube responds elastically but exhibits a larger bond distortion (up to 5.5%) for the atoms in the region underneath the tip than the global strain ($\leq 0.7\%$). This distortion accounts for the initial conductance decrease at small bending angles where the overall simulated structure remains sp^2. As tip-pushing proceeds, the tube structure progressively evolves and larger structural changes occur underneath the tip. The average number of bonds per atom in the tube section proximal to the tip has increased from 3 to ~3.3 for deflection angle $\theta = 11°$ ($\sigma = 1.8\%$) and to 3.6 for $\theta = 15°$ ($\sigma = 3.4\%$). This indicates that the local bonding configuration has changed from sp^2 to nearly sp^3. Away from the tip region, the nanotube remains essentially in a sp^2-bonding configuration with bond deformation characterized by the global strain parameter σ. Further local analysis[17] of the bent nanotube in the tip vicinity reveals the onset of an increase in σ-electrons contributing to the local density of states at the Fermi level in the highly deformed local region. This is, however, accompanied by a significant decrease in the π-electron density. As the π-electrons are delocalized and therefore mainly responsible for electrical conduction, a drastic reduction in the π-electron density is responsible for the substantial decrease in conductance. Simulations also find that the local and global deformations of the nanotube are highly reversible (for $\theta < 15°$, $\sigma < 3.4\%$) upon moving the tip away, leading to the recovery of the nanotube structure and electrical conductance. These results are in excellent agreement with our experimental observations.

The deviation of force versus deflection $F(\delta)$ curve from the δ^3-relation for $\sigma > \sim 0.3\%$ ($\theta > \sim 5°$, Fig. 2) should be owing to large local-strain developed in the sp^3 region proximal to the tip, as the elastic string model assuming a homogeneous global strain becomes invalid. This is consistent with the electromechanical behaviour that beyond the elastic response regime ($\theta > \sim 5°$, Fig. 4a, inset), tip-forced sp^3 bonding within the nanotube occurs, causing a significant decrease in the nanotube conductance.

Previous theoretical investigations indicate that the electrical properties of metallic SWNTs should be insensitive to small bending deformations[2,4,18]. The calculated conductance of a (5,5) SWNT changes very little for bending angles up to $\theta = 24°$, when bending at the centre of the SWNT is modelled by holding the ends of the tube at fixed positions to define the bending angle without the involvement of a tip[3]. This results in a situation where the atomic bonding characteristics of the bent nanotube still remain sp^2. The absence of sp^3 bonding in the simulated structure should account for the small electrical conductance change[3]. A similar bending technique[18] found that the electrical conductance of a metallic (6,6) SWNT did not change significantly for bending angles up to $\theta \sim 22.5°$. At larger bending angles (for example $\theta = 45°$) the conductance of the SWNT was lowered by at most tenfold. The conductance decrease is explained by σ–π hybridization effects owing to the increased curvature under high bending angles[18].

Here we used an AFM tip both in experiments and in simulations, a key to performing the experimental measurements and obtaining a fundamental understanding. Our work elucidates the electromechanical properties of the nanotube when mechanical action of a local probe causes a large local deformation. This differs from previous considerations of deformed nanotubes in which the nanotube structure is more or less uniformly bent or strained (at least in the bending-angle range investigated here). The experimental investigation of uniform global strain or bending effects requires different nanotube manipulation mechanisms, such as electrostatic forces[19]. We believe that the physics presented here should hold for SWNTs containing large local deformations caused by other forces. For instance, if a highly kinked SWNT stabilized by van der Waals forces on a substrate develops sp^3 bonding characteristics at the kink, the electrical conductance should be significantly reduced compared to a straight tube. □

Received 8 December 1999; accepted 20 April 2000.

1. Crespi, V., Cohen, M. & Rubio, A. *In situ* band gap engineering of carbon nanotubes. *Phys. Rev. Lett.* **79,** 2093–2096 (1997).
2. Kane, C. L. & Mele, E. J. Size, shape, and low energy electronic structure of carbon nanotubes. *Phys. Rev. Lett.* **78,** 1932–1935 (1997).
3. Nardelli, M. & Bernholc, J. Mechanical deformations and coherent transport in carbon nanotubes. *Phys. Rev. B,* **60,** R16338–16341 (1998).
4. Rochefort, A., Salahub, D. & Avouris, P. The effect of structural distortions on the electronic structure of carbon nanotubes. *Chem. Phys. Lett.* **297,** 45–50 (1998).
5. Bezryadin, A., Verschueren, A., Tans, S. & Dekker, C. Multiprobe transport experiments on individual single-wall carbon nanotubes. *Phys. Rev. Lett.* **80,** 4036–4039 (1998).
6. Paulson, S. *et al. In situ* resistance measurements of strained carbon nanotubes. *Appl. Phys. Lett.* **75,** 2936–2938 (1999).
7. Kong, J., Soh, H., Cassell, A., Quate, C. F. & Dai, H. Synthesis of individual single-walled carbon nanotubes on patterned silicon wafers. *Nature* **395,** 878–881 (1998).
8. Soh, H. *et al.* Integrated nanotube circuits: controlled growth and ohmic contacting of single-walled carbon nanotubes. *Appl. Phys. Lett.* **75,** 627–629 (1999).
9. Kong, J. *et al.* Synthesis, integration and electrical properties of individual single-walled carbon nanotubes. *Appl. Phys. A* **69,** 305–308 (1999).
10. Salvetat, J. P. *et al.* Elastic and shear moduli of single-walled carbon nanotube ropes. *Phys. Rev. Lett.* **82,** 944–947 (1999).
11. Timoshenko, S. *Strength of Materials. Part I, Elementary Theory and Problems* (Van Nostrand, New York, 1930).
12. Walters, D. *et al.* Elastic strain of freely suspended single-walled carbon nanotube ropes. *Appl. Phys. Lett.* **74,** 3803–3805 (1999).
13. Hertel, T., Martel, R. & Avouris, P. Manipulation of individual carbon nanotubes and their interaction with surfaces. *J. Phys. Chem.* **102,** 910–915 (1998).
14. Jayanthi, C. S. *et al.* Order-N method for a nonorthogonal tight-binding Hamiltonian. *Phys. Rev. B* **57,** 3799–3802 (1998).
15. Datta, S. *Electronic Transport in Mesoscopic Systems.* (University Press, Cambridge, 1995).
16. Wu, S. Y. & Jayanthi, C. S. Local analysis via the real space greens function method. *J. Modern Phys. B* **9,** 1869–1897 (1995).
17. Alfonso, D., Wu, S. Y., Jayanthi, C. S. & Kaxiras, E. Linking chemical reactivity, magic numbers, and local electronic properties of clusters. *Phys. Rev. B* **59,** 7745–7750 (1999).
18. Rochefort, A., Lesage, F., Salhub, D. & Avouris, P. Conductance of distorted carbon nanotubes. *Phys. Rev. B.* **60,** 13824–13830 (1999).
19. Kim, P. & Lieber, C. Nanotube nanotweezers. *Science* **286,** 2148–2150 (1999).

Acknowledgements

We thank C. Quate for discussions and use of equipment. This work was supported by the Defense Advanced Research Projects Agency/Office of Naval Research, National Science Foundation, Semiconductor Research Corporation/Motorola, a David and Lucile Packard Fellowship, a Terman Fellowship, the Laboratory for Advance Materials at Stanford, National Nanofabrication Users Network at Stanford, the Camile Henry-Dreyfus Foundation, the American Chemical Society and the University of Kentucky Center for Computer Sciences.

Correspondence and requests for materials should be addressed to H.D. (email: hdai@chem.stanford.edu).

Controlling droplet deposition with polymer additives

Vance Bergeron†, Daniel Bonn‡, Jean Yves Martin† & Louis Vovelle†

† *Rhodia Recherches, Centre de Recherches Lyon, 85 Av. Des Freres Perret-BP62, 69192 Saint-Fons Cedex, France*
‡ *Ecole Normale Superieure, Laboratoire de Physique Statistique, 24 rue Lhomond, 75231 Paris Cedex 05, France*

Controlling the impact of drops onto solid surfaces is important for a wide variey of coating and deposition processes—for example, the treatment of plants with herbicides and pesticides requires precise targeting in order to meet stringent toxicological regulations. However, the outer wax-like layer of the leaves is a non-wetting substrate that causes sprayed droplets to rebound; often less than 50% of the initial spray is retained by the plant[1]. Although the impact and subsequent retraction of non-wetting aqueous drops on a hydrophobic surface have been the subjects of